1-2000

# Study of charm production in Z decays

R. BARATE

M. THULASIDAS
*Singapore Management University*, manojt@smu.edu.sg

EUROPEAN LABORATORY FOR PARTICLE PHYSICS

**CERN/EP 99-094**
July 8, 1999

# Study of Charm Production in Z Decays

The ALEPH collaboration*

## Abstract

The production rates of $D^{*\pm}$, $D_s^{*\pm}$, $D^{\pm}$, $D^0/\bar{D}^0$, $D_s^{\pm}$, and $\Lambda_c^+/\bar{\Lambda}_c^-$ in $Z \to c\bar{c}$ decays are measured using the LEP I data sample recorded by the ALEPH detector. The fractional energy spectrum of the $D^{*\pm}$ is well described as the sum of three contributions: charm hadronisation, b hadron decays and gluon splitting into a pair of heavy quarks. The probability for a c quark to hadronise into a $D^{*+}$ is found to be $f(c \to D^{*+}) = 0.233 \pm 0.010(\text{stat.}) \pm 0.011(\text{syst.})$. The average fraction of the beam energy carried by $D^{*\pm}$ mesons in $Z \to c\bar{c}$ events is measured to be $\langle X_E(D^{*\pm})\rangle_{c\bar{c}} = 0.4878 \pm 0.0046(\text{stat.}) \pm 0.0061(\text{syst.})$. The $D^{*\pm}$ energy and the hemisphere mass imbalance distributions are simultaneously used to measure the fraction of hadronic Z decays in which a gluon splits to a $c\bar{c}$ pair: $\bar{n}_{g\to c\bar{c}} = (3.23 \pm 0.48(\text{stat.}) \pm 0.53(\text{syst.}))\%$. The ratio of the Vector/(Vector+Pseudoscalar) production rates in charmed mesons is found to be $P_V = 0.595 \pm 0.045$. The fractional decay width of the Z into $c\bar{c}$ pairs is determined from the sum of the production rates for various weakly decaying charmed states to be $R_c = 0.1738 \pm 0.0047(\text{stat.}) \pm 0.0116(\text{syst.})$.

(Submitted to the European Physical Journal C)

* See next pages for the list of authors.

# The ALEPH Collaboration

R. Barate, D. Decamp, P. Ghez, C. Goy, J.-P. Lees, E. Merle, M.-N. Minard, B. Pietrzyk

*Laboratoire de Physique des Particules (LAPP), IN$^2$P$^3$-CNRS, F-74019 Annecy-le-Vieux Cedex, France*

R. Alemany, M.P. Casado, M. Chmeissani, J.M. Crespo, E. Fernandez, M. Fernandez-Bosman, Ll. Garrido,[15] E. Graugès, A. Juste, M. Martinez, G. Merino, R. Miquel, Ll.M. Mir, A. Pacheco, I.C. Park, I. Riu

*Institut de Física d'Altes Energies, Universitat Autònoma de Barcelona, E-08193 Bellaterra (Barcelona), Spain*[7]

A. Colaleo, D. Creanza, M. de Palma, G. Iaselli, G. Maggi, M. Maggi, S. Nuzzo, A. Ranieri, G. Raso, F. Ruggieri, G. Selvaggi, L. Silvestris, P. Tempesta, A. Tricomi,[3] G. Zito

*Dipartimento di Fisica, INFN Sezione di Bari, I-70126 Bari, Italy*

X. Huang, J. Lin, Q. Ouyang, T. Wang, Y. Xie, R. Xu, S. Xue, J. Zhang, L. Zhang, W. Zhao

*Institute of High-Energy Physics, Academia Sinica, Beijing, The People's Republic of China*[8]

D. Abbaneo, U. Becker,[19] G. Boix,[6] M. Cattaneo, F. Cerutti, V. Ciulli, G. Dissertori, H. Drevermann, R.W. Forty, M. Frank, T.C. Greening, A.W. Halley, J.B. Hansen, J. Harvey, P. Janot, B. Jost, I. Lehraus, O. Leroy, P. Mato, A. Minten, A. Moutoussi, F. Ranjard, L. Rolandi, D. Schlatter, M. Schmitt,[20] O. Schneider,[2] P. Spagnolo, W. Tejessy, F. Teubert, I.R. Tomalin, E. Tournefier, A.E. Wright

*European Laboratory for Particle Physics (CERN), CH-1211 Geneva 23, Switzerland*

Z. Ajaltouni, F. Badaud, G. Chazelle, O. Deschamps, A. Falvard, C. Ferdi, P. Gay, C. Guicheney, P. Henrard, J. Jousset, B. Michel, S. Monteil, J-C. Montret, D. Pallin, P. Perret, F. Podlyski

*Laboratoire de Physique Corpusculaire, Université Blaise Pascal, IN$^2$P$^3$-CNRS, Clermont-Ferrand, F-63177 Aubière, France*

J.D. Hansen, J.R. Hansen, P.H. Hansen, B.S. Nilsson, B. Rensch, A. Wäänänen

*Niels Bohr Institute, DK-2100 Copenhagen, Denmark*[9]

G. Daskalakis, A. Kyriakis, C. Markou, E. Simopoulou, I. Siotis, A. Vayaki

*Nuclear Research Center Demokritos (NRCD), GR-15310 Attiki, Greece*

A. Blondel, G. Bonneaud, J.-C. Brient, A. Rougé, M. Rumpf, M. Swynghedauw, M. Verderi, H. Videau

*Laboratoire de Physique Nucléaire et des Hautes Energies, Ecole Polytechnique, IN$^2$P$^3$-CNRS, F-91128 Palaiseau Cedex, France*

E. Focardi, G. Parrini, K. Zachariadou

*Dipartimento di Fisica, Università di Firenze, INFN Sezione di Firenze, I-50125 Firenze, Italy*

R. Cavanaugh, M. Corden, C. Georgiopoulos

*Supercomputer Computations Research Institute, Florida State University, Tallahassee, FL 32306-4052, USA* [13,14]

A. Antonelli, G. Bencivenni, G. Bologna,[4] F. Bossi, P. Campana, G. Capon, V. Chiarella, P. Laurelli, G. Mannocchi,[1,5] F. Murtas, G.P. Murtas, L. Passalacqua, M. Pepe-Altarelli[1]

*Laboratori Nazionali dell'INFN (LNF-INFN), I-00044 Frascati, Italy*

L. Curtis, J.G. Lynch, P. Negus, V. O'Shea, C. Raine, P. Teixeira-Dias, A.S. Thompson

*Department of Physics and Astronomy, University of Glasgow, Glasgow G12 8QQ,United Kingdom*[10]

O. Buchmüller, S. Dhamotharan, C. Geweniger, G. Graefe, P. Hanke, G. Hansper, V. Hepp, E.E. Kluge, A. Putzer, J. Sommer, K. Tittel, S. Werner,[19] M. Wunsch

*Institut für Hochenergiephysik, Universität Heidelberg, D-69120 Heidelberg, Germany*[16]

R. Beuselinck, D.M. Binnie, W. Cameron, P.J. Dornan,[1] M. Girone, S. Goodsir, E.B. Martin, N. Marinelli, A. Sciabà, J.K. Sedgbeer, E. Thomson, M.D. Williams

*Department of Physics, Imperial College, London SW7 2BZ, United Kingdom*[10]

V.M. Ghete, P. Girtler, E. Kneringer, D. Kuhn, G. Rudolph

*Institut für Experimentalphysik, Universität Innsbruck, A-6020 Innsbruck, Austria*[18]

C.K. Bowdery, P.G. Buck, A.J. Finch, F. Foster, G. Hughes, R.W.L. Jones, N.A. Robertson, M.I. Williams

*Department of Physics, University of Lancaster, Lancaster LA1 4YB, United Kingdom*[10]

I. Giehl, K. Jakobs, K. Kleinknecht, G. Quast, B. Renk, E. Rohne, H.-G. Sander, H. Wachsmuth, C. Zeitnitz

*Institut für Physik, Universität Mainz, D-55099 Mainz, Germany*[16]

J.J. Aubert, C. Benchouk, A. Bonissent, J. Carr,[1] P. Coyle, F. Etienne, F. Motsch, P. Payre, D. Rousseau, M. Talby, M. Thulasidas

*Centre de Physique des Particules, Faculté des Sciences de Luminy, IN$^2$P$^3$-CNRS, F-13288 Marseille, France*

M. Aleppo, M. Antonelli, F. Ragusa

*Dipartimento di Fisica, Università di Milano e INFN Sezione di Milano, I-20133 Milano, Italy*

V. Büscher, H. Dietl, G. Ganis, K. Hüttmann, G. Lütjens, C. Mannert, W. Männer, H.-G. Moser, S. Schael, R. Settles, H. Seywerd, H. Stenzel, W. Wiedenmann, G. Wolf

*Max-Planck-Institut für Physik, Werner-Heisenberg-Institut, D-80805 München, Germany*[16]

P. Azzurri, J. Boucrot, O. Callot, S. Chen, A. Cordier, M. Davier, L. Duflot, J.-F. Grivaz, Ph. Heusse, A. Jacholkowska,[1] F. Le Diberder, J. Lefrançois, A.-M. Lutz, M.-H. Schune, J.-J. Veillet, I. Videau,[1] D. Zerwas

*Laboratoire de l'Accélérateur Linéaire, Université de Paris-Sud, IN$^2$P$^3$-CNRS, F-91898 Orsay Cedex, France*

G. Bagliesi, S. Bettarini, T. Boccali, C. Bozzi,[12] G. Calderini, R. Dell'Orso, I. Ferrante, L. Foà, A. Giassi, A. Gregorio, F. Ligabue, A. Lusiani, P.S. Marrocchesi, A. Messineo, F. Palla, G. Rizzo, G. Sanguinetti, G. Sguazzoni, R. Tenchini, C. Vannini, A. Venturi, P.G. Verdini

*Dipartimento di Fisica dell'Università, INFN Sezione di Pisa, e Scuola Normale Superiore, I-56010 Pisa, Italy*

G.A. Blair, G. Cowan, M.G. Green, T. Medcalf, J.A. Strong, J.H. von Wimmersperg-Toeller

*Department of Physics, Royal Holloway & Bedford New College, University of London, Surrey TW20 OEX, United Kingdom*[10]

D.R. Botterill, R.W. Clifft, T.R. Edgecock, P.R. Norton, J.C. Thompson

*Particle Physics Dept., Rutherford Appleton Laboratory, Chilton, Didcot, Oxon OX11 OQX, United Kingdom*[10]

B. Bloch-Devaux, P. Colas, S. Emery, W. Kozanecki, E. Lançon, M.-C. Lemaire, E. Locci, P. Perez, J. Rander, J.-F. Renardy, A. Roussarie, J.-P. Schuller, J. Schwindling, A. Trabelsi,[21] B. Vallage

*CEA, DAPNIA/Service de Physique des Particules, CE-Saclay, F-91191 Gif-sur-Yvette Cedex, France*[17]

S.N. Black, J.H. Dann, R.P. Johnson, H.Y. Kim, N. Konstantinidis, A.M. Litke, M.A. McNeil, G. Taylor

*Institute for Particle Physics, University of California at Santa Cruz, Santa Cruz, CA 95064, USA*[22]

C.N. Booth, S. Cartwright, F. Combley, M.S. Kelly, M. Lehto, L.F. Thompson

*Department of Physics, University of Sheffield, Sheffield S3 7RH, United Kingdom*[10]

K. Affholderbach, A. Böhrer, S. Brandt, C. Grupen, J. Hess, C. Koob, A. Misiejuk, G. Prange, U. Sieler

*Fachbereich Physik, Universität Siegen, D-57068 Siegen, Germany*[16]

G. Giannini, B. Gobbo

*Dipartimento di Fisica, Università di Trieste e INFN Sezione di Trieste, I-34127 Trieste, Italy*

J. Rothberg, S. Wasserbaech

*Experimental Elementary Particle Physics, University of Washington, WA 98195 Seattle, U.S.A.*

S.R. Armstrong, P. Elmer, D.P.S. Ferguson, Y. Gao, S. González, O.J. Hayes, H. Hu, S. Jin, P.A. McNamara III, J. Nielsen, W. Orejudos, Y.B. Pan, Y. Saadi, I.J. Scott, J. Walsh, Sau Lan Wu, X. Wu, G. Zobernig

*Department of Physics, University of Wisconsin, Madison, WI 53706, USA*[11]

[1]Also at CERN, 1211 Geneva 23, Switzerland.

[2]Now at Université de Lausanne, 1015 Lausanne, Switzerland.

[3]Also at Centro Siciliano di Fisica Nucleare e Struttura della Materia, INFN, Sezione di Catania, 95129 Catania, Italy.

[4]Also Istituto di Fisica Generale, Università di Torino, 10125 Torino, Italy.

[5]Also Istituto di Cosmo-Geofisica del C.N.R., Torino, Italy.

[6]Supported by the Commission of the European Communities, contract ERBFMBICT982894.

[7]Supported by CICYT, Spain.

[8]Supported by the National Science Foundation of China.

[9]Supported by the Danish Natural Science Research Council.

[10]Supported by the UK Particle Physics and Astronomy Research Council.

[11]Supported by the US Department of Energy, grant DE-FG0295-ER40896.

[12]Now at INFN Sezione de Ferrara, 44100 Ferrara, Italy.

[13]Supported by the US Department of Energy, contract DE-FG05-92ER40742.

[14]Supported by the US Department of Energy, contract DE-FC05-85ER250000.

[15]Permanent address: Universitat de Barcelona, 08208 Barcelona, Spain.

[16]Supported by the Bundesministerium für Bildung, Wissenschaft, Forschung und Technologie, Germany.

[17]Supported by the Direction des Sciences de la Matière, C.E.A.

[18]Supported by Fonds zur Förderung der wissenschaftlichen Forschung, Austria.

[19]Now at SAP AG, 69185 Walldorf, Germany.

[20]Now at Harvard University, Cambridge, MA 02138, U.S.A.

[21]Now at Département de Physique, Faculté des Sciences de Tunis, 1060 Le Belvédère, Tunisia.

[22]Supported by the US Department of Energy, grant DE-FG03-92ER40689.

# 1 Introduction

Charm quarks are produced in 40% of the hadronic Z decays, mostly coming from $Z \to c\bar{c}$ or $b\bar{b}$, but also from gluon splitting to $c\bar{c}$ or $b\bar{b}$. This paper presents a wide-ranging survey of the production of the weakly decaying charm states $D^0$, $D^+$, $D_s^+$ mesons and $\Lambda_c^+$ baryons and the first excited states $D^{*+}$, $D_s^{*+}$ in Z decays (here and throughout this paper, charge conjugation is implied). It extends the work of previous publications [1, 2] to the full data sample collected by ALEPH between 1991 and 1995, which consists of four million hadronic Z decays. A new algorithm based on the mass of particles from secondary vertices greatly improves the separation of charm states resulting from $b\bar{b}$ and $c\bar{c}$ production.

The paper is organised as follows. After a brief description of relevant details of the ALEPH detector in Section 2, the procedures adopted to reconstruct the above charm states are given in Section 3. The cleanest charm signal is obtained for the $D^{*+}$ mesons and Section 4 is devoted to the fractional energy spectrum for their production, which now covers the whole range from 0.1 to 1.0, and the relative strengths of the $b\bar{b}$, $c\bar{c}$ and gluon splitting components. In Section 5 a new technique involving the heavy and light hemisphere masses is introduced in order to obtain a more accurate measure of the rate for gluon splitting to charm quarks. A measurement of the $D_s^{*\pm}$ production rate is given in Section 6. Determinations of the production rates for the weakly decaying charm states are presented in Section 7 and this information is used in Section 8 to yield a measurement of $R_c = \Gamma(Z \to c\bar{c})/\Gamma(Z \to \mathit{hadrons})$ from charm counting.

# 2 The ALEPH detector

A detailed description of the ALEPH detector and its performance can be found in Refs. [3, 4]. Only a brief review is given here.

Charged particles are detected in the central part, consisting of a two-layer silicon vertex detector with double-sided ($r$-$\phi$ and $z$) readout, a cylindrical drift chamber and a large time projection chamber (TPC), which together measure up to 33 coordinates along the charged particle trajectories. Tracking is performed in a 1.5 T magnetic field provided by a superconducting solenoid. For high momentum tracks the combined system yields a $1/p_T$ resolution of $6 \times 10^{-4}(\mathrm{GeV}/c)^{-1}$ and an impact parameter resolution of 25 $\mu$m in both the $r$-$\phi$ and $z$ projections. The TPC also provides up to 338 measurements of ionization ($dE/dx$) allowing particle identification to be performed. For tracks having at least 50 energy deposition measurements, the variable $\chi_h$ is defined as $(I_{\mathrm{meas}} - I_h)/\sigma_h$, where $I_{\mathrm{meas}}$ is the measured value of $dE/dx$, $I_h$ is the expected value for particle type $h$ ($h = \mathrm{p}, \mathrm{K}$ or $\pi$), and $\sigma_h$ is the expected uncertainty.

Data from the vertex detector is particularly important for b tagging for which a lifetime-mass algorithm has been designed to provide discrimination between b quarks and lighter quarks. This algorithm uses the significance $\mathcal{S}$ of the three-dimensional impact parameter for each charged track to define the confidence level for it to be consistent with coming from the primary vertex. These confidence levels are combined to obtain the confidence level $\mathcal{P}_{\mathcal{H}}$ for all tracks of an hemisphere to come from the primary vertex. The distribution of $\mathcal{P}_{\mathcal{H}}$ is strongly peaked near zero for b hemispheres. A second b tagging variable makes use of the b/c hadron mass difference: the tracks

in a hemisphere are grouped together in order of decreasing $\mathcal{S}$ until an effective mass of 1.8 GeV/$c^2$ is reached for the system, and the confidence level $\mu_{\mathcal{H}}$ for the last added track to come from the primary vertex is used as the tagging variable. This is peaked at zero for b quarks. These two tagging variables are combined in a single one: $\mathcal{B}_{tag} = -(0.7log_{10}\mu_{\mathcal{H}} + 0.3log_{10}\mathcal{P}_{\mathcal{H}}$. A detailed description of this algorithm can be found in Ref. [5].

The electromagnetic calorimeter is a lead/wire-chamber sandwich operated in proportional mode. It is read out in projective towers of typically $15 \times 15$ mrad$^2$ size segmented in three longitudinal sections. The iron return yoke is instrumented with streamer tubes read out in projective towers and this provides the hadron calorimetry.

The tracking and calorimetry information is combined in an energy flow algorithm providing a list of objects classified as tracks, photons and neutral hadrons. Particle tracks which originate from within a cylinder of 2 cm radius and 20 cm length centred on the nominal interaction point, and which have more than 4 TPC hits, are defined as *good tracks*. Hadronic Z decays are selected by requiring the presence of at least 5 such good tracks and a total visible energy greater than 10% of the centre-of-mass energy [6].

# 3 Reconstruction of Charmed Hadron Decays

Each charm hadron species is reconstructed in the decay mode best suited to a rate measurement, i.e. with a large enough and accurately known branching ratio, and a sufficiently low background.

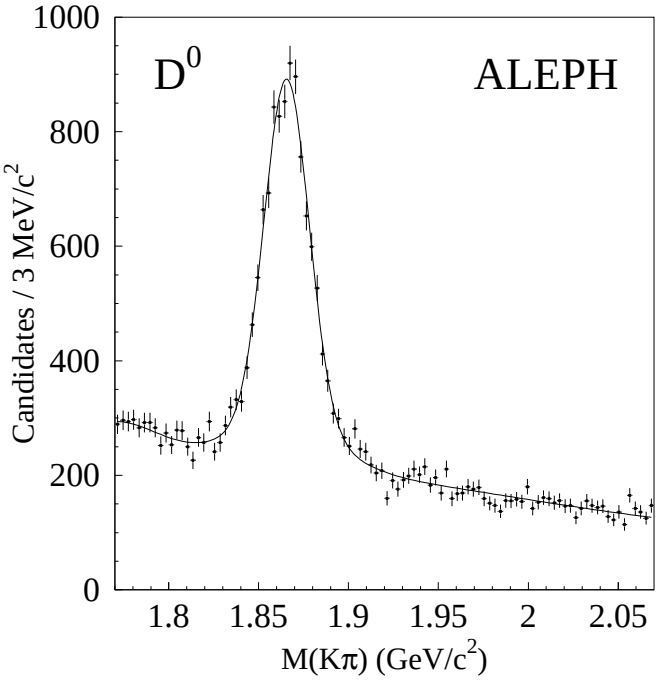


Figure 1: $K^-\pi^+$ invariant mass distribution. The fitted curve is described in section 7.

### 3.1 $D^0$ Meson

$D^0$ mesons are selected through their decay mode $D^0 \to K^-\pi^+$. A track with a momentum greater than 2.5 GeV/$c$, to which the kaon mass is assigned, is combined with a track of opposite charge with a momentum greater than 1.5 GeV/$c$, which is assumed to be a pion. The contribution due to wrong mass assignment of the two tracks from the $D^0$ is reduced by means of the $dE/dx$ measurement of the kaon candidate when available. The $dE/dx$ of the kaon track must be closer to the expectation for a kaon than that for a pion: $|\chi_K| < |\chi_\pi|$. The pair formed by the two tracks is retained if its fractional energy $X_E = E/E_{\rm beam}$ is greater than 0.5 and if a common vertex with a $\chi^2$ probability greater than 1% is found. The significance of the $D^0$ decay length, projected on the $D^0$ momentum, is required to be greater than 1. The invariant mass distribution is shown in Fig. 1.

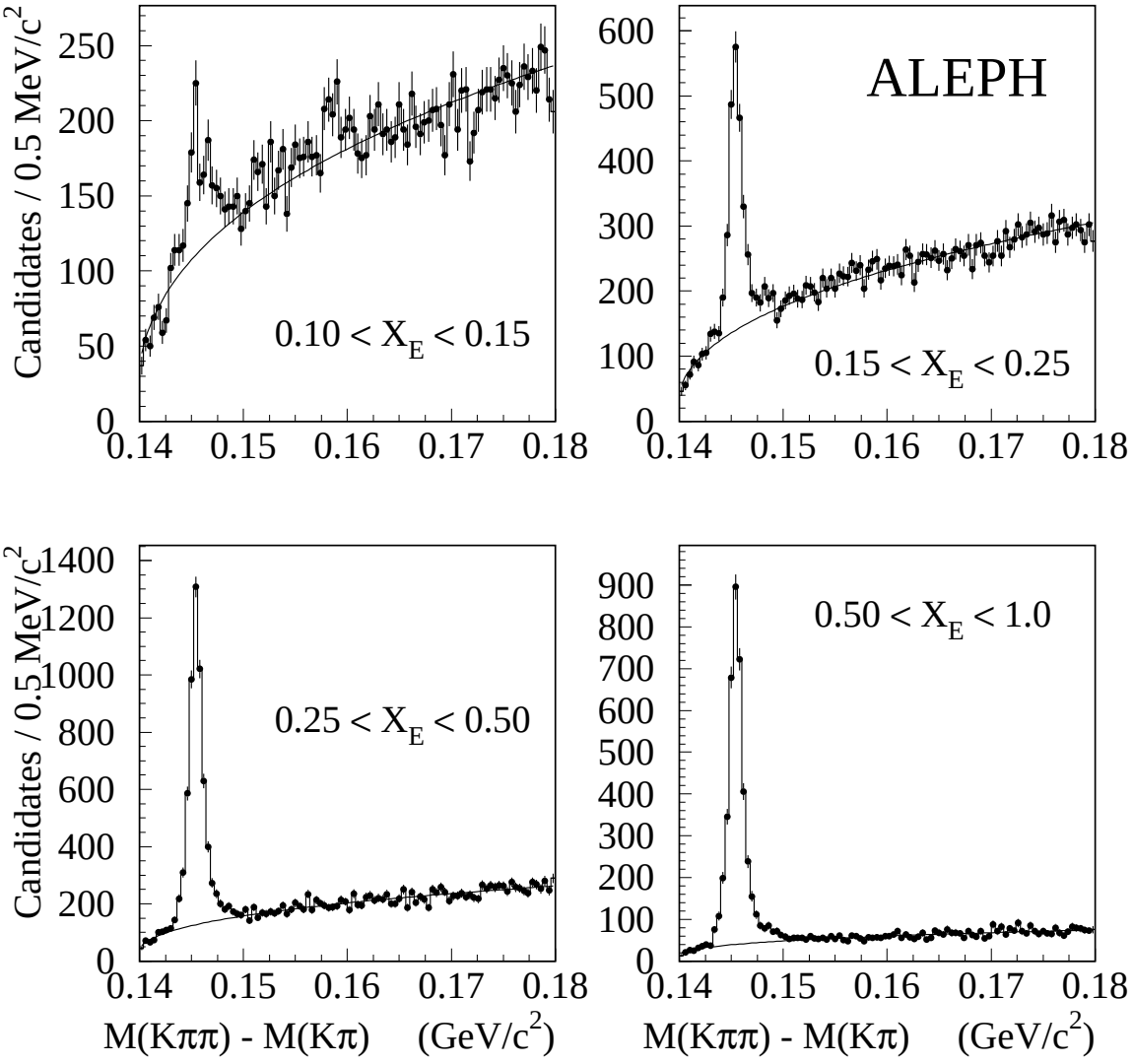


Figure 2: Distribution of the $K\pi\pi$ - $K\pi$ mass difference in four different ranges of the $K\pi\pi$ energy, after requiring that the $K\pi$ mass is consistent with the $D^0$ mass (histogram with error bars). The background fit is also shown.

## 3.2 $D^{*+}$ Meson

The $D^{*+} \to D^0\pi^+$, $D^0 \to K^-\pi^+$ decay chain is reconstructed by considering triplets of charged tracks with total charge $\pm 1$. The pion mass is assigned to the two particles with the same charge, and the kaon mass to the remaining one. The total energy of the triplet is required to be greater than $0.1 \times E_{\rm beam}$. Any $K^-\pi^+$ combination whose mass is within 30 MeV/$c^2$ of the $D^0$ mass is kept. For such a combination, the mass difference $M(K\pi\pi) - M(K\pi)$ is calculated and required to be within 1.6 MeV/$c^2$ of the nominal $D^{*+} - D^0$ mass difference. The combinatorial background level is a steeply falling function of $X_E$ and background rejection must therefore be enhanced as one goes to lower $X_E$. For this, the scalar nature of the $D^0$ and its significant lifetime are used as follows. The distribution of the cosine of the $D^0$ decay angle (defined in the $K\pi$ rest frame as the angle $\theta^*$ of the kaon with the $K\pi$ line of flight in the laboratory) is isotropic, whereas the background peaks forward and backward, and so, for $X_E < 0.45$ it is required that $-0.8 < \cos\theta^* < 0.9$. The decay length significance is required to be positive for $0.3 < X_E < 0.4$ and greater than 1 for $X_E$ less than 0.3. The $\chi^2$ probability for the secondary vertex fit is required to be greater than 1% for $X_E < 0.15$. The mass-difference distributions in four $X_E$ ranges are shown in Fig. 2.

## 3.3 $D^+$ Meson

The $D^+$ meson is reconstructed in the decay mode $D^+ \to K^-\pi^+\pi^+$. Combinations of three tracks are formed with the same mass assignment as for the $D^{*+}$ reconstruction. To fight the high background of this decay, the kaon track candidate is required to have a momentum greater than 2.5 GeV/$c$ and an associated $dE/dx$ satisfying $\chi_K + \chi_\pi < 1$, one of the two pion tracks must have a momentum greater than 1.5 GeV/$c$, while the other must have more than 0.75 GeV/$c$. Both of the possible $K\pi$ combinations are required to have a $K\pi\pi$-$K\pi$ mass difference larger than 0.15 GeV/$c^2$, in order to reject candidates consistent with the decay $D^{*+} \to \pi^+D^0 \to \pi^+K^-\pi^+X$. Triplets of tracks with a total energy greater than $0.5 \times E_{\rm beam}$ and forming a common vertex with a $\chi^2$ probability greater than 1% are retained. A projected decay length significance greater than 1.5 is required for the reconstructed $D^+$ vertices. The invariant mass distribution is shown in Fig. 3.

## 3.4 $D_s^+$ Meson

The $D_s^+$ is reconstructed in the decay chain $D_s^+ \to \phi\pi^+$ with a subsequent decay $\phi \to K^+K^-$. The kaon momenta must exceed 1.5 GeV/$c$ and the pion momentum must be greater than 2.5 GeV/$c$. The kaon candidates are required to have $dE/dx$ information available and to fulfill $\chi_K + \chi_\pi < 1$. In addition all tracks for which $dE/dx$ is available must satisfy $|\chi_x| < 2.5$ for the given particle hypothesis. If $|M_{KK} - M_\phi| < 5$ GeV/$c^2$ and $p_\phi > 4$ GeV/$c$ the candidate is kept and the three particles fitted to a common vertex. Candidates with a $\chi^2$ greater than 15 (there are 3 degrees of freedom) are rejected. A cut on $|\cos\lambda^*| > 0.4$, where $\lambda^*$ is the angle between the kaon and the pion in the $\phi$ rest frame, motivated by the $P$-wave nature of the $\phi$ decay, strongly suppresses the background. The mass distribution of the $D_s^+$ candidates is shown in Fig. 4.

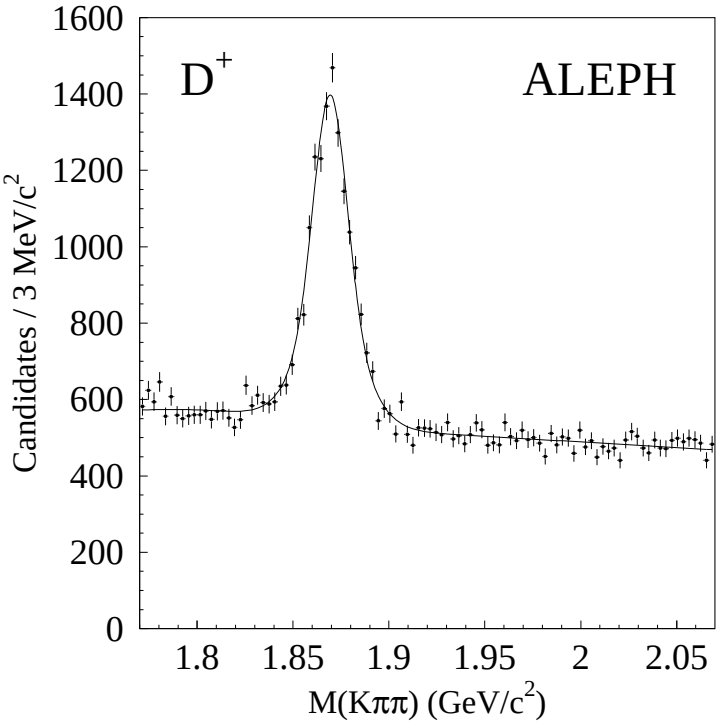


Figure 3: $K^-\pi^+\pi^+$ invariant mass distribution with the fit result.

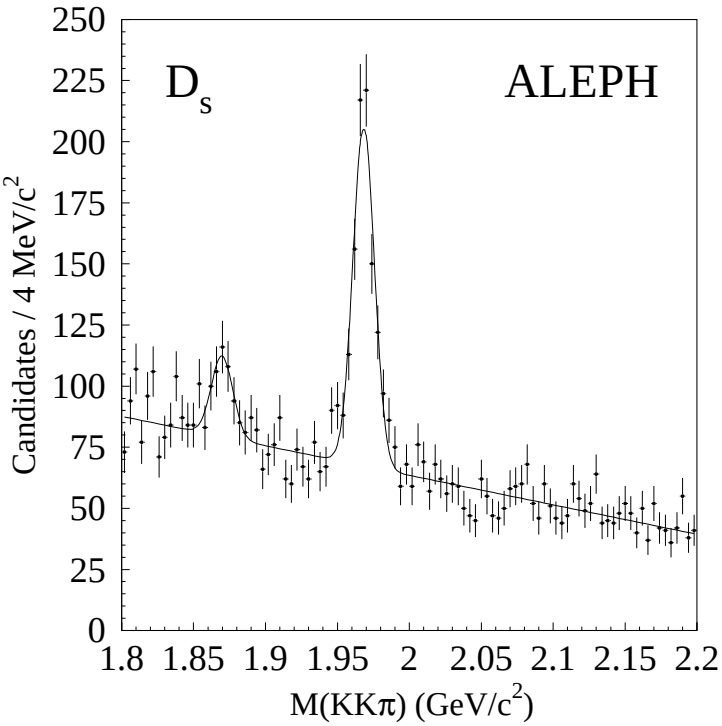


Figure 4: $K^+K^-\pi^+$ invariant mass distribution, with the fit result. The peak at low mass comes from the $D^+$

### 3.5 $D_s^{*+}$ Meson

The $D_s^{*+}$ meson is reconstructed in the decay channel $D_s^{*+} \to D_s^+\gamma$, followed by $D_s^+ \to K^+K^-\pi^+$ through either the $\phi\pi^+$ or the $\bar{K}^{*0}K^+$ decay mode.

In the $D_s^+$ reconstruction, tracks are taken as kaon candidates when the $dE/dx$ measurement satisfies $|\chi_K| < |\chi_\pi|$, and as pion candidates when $|\chi_K| > |\chi_\pi|$. To select the $D_s^+$ mesons decaying into $\phi\pi^+$, pairs of opposite-charge kaon candidates satisfying $|M_{KK} - M_\phi| < 8$ MeV/$c^2$ are required to form a vertex with a pion candidate with a probability greater than 1% and $|\cos\lambda^*|$ greater than 0.4. $D_s^+$ candidates decaying into $\bar{K}^*K$ are selected when kaon and pion candidates with opposite charges fulfill $|M_{K\pi} - M_{K^*}| < 25$ MeV/$c^2$ and $|\cos\lambda^*| > 0.6$.

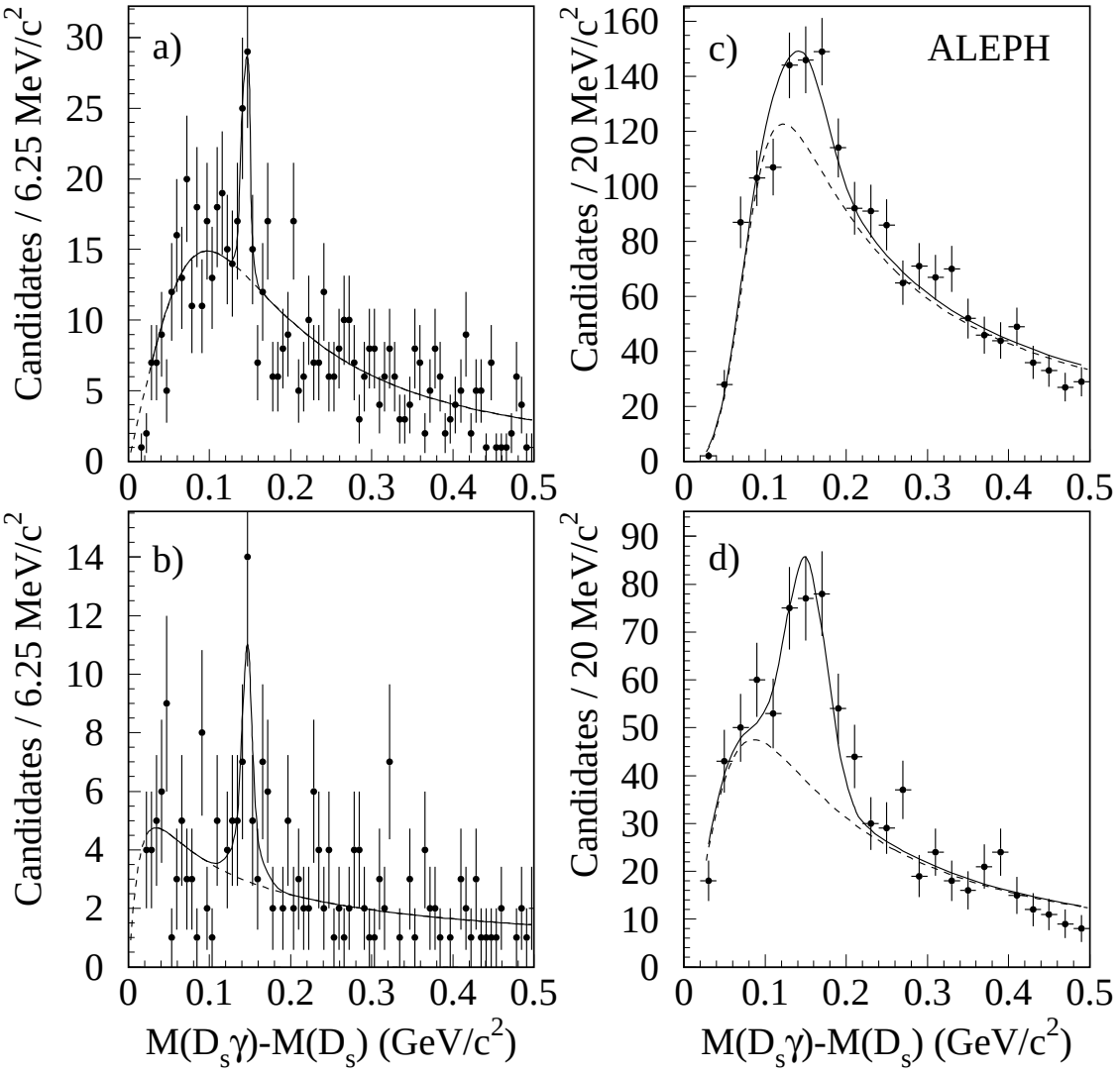


Figure 5: $M(D_s^{*+}) - M(D_s^+)$ distributions with conversions in the $b\bar{b}$-enriched sample (a) and in the $c\bar{c}$-enriched sample (b), and with calorimetric photons (c), (d). The binnings have been chosen to match the different resolutions in the two photon detection methods. The dashed line is the background fit described in Section 6

Photon candidates for the $D_s^{*+}$ are selected when they have an energy greater than 0.6 GeV in the electromagnetic calorimeter and do not form a $\pi^0$ candidate. Photon

conversions in the detector are identified by searching for electron tracks that are geometrically consistent with the conversion hypothesis. To increase the efficiency for converted photons, electron-positron pairs where one track is not detected are also identified, as described in [7]. Photon conversion candidates must have an energy larger than 0.3 GeV to be taken into account.

To be able to measure separately the production rate of $\mathrm{D_s^{*+}}$ mesons in $\mathrm{c\bar{c}}$ and $\mathrm{b\bar{b}}$ events, two different subsamples of $\mathrm{D_s^{*+}}$ candidates are selected. One subsample is enriched in $\mathrm{b\bar{b}}$ events and consists of $\mathrm{D_s^{*+}}$ candidates with a $\mathrm{D_s^+}$ momentum 8 GeV/$c$ $< p_{\mathrm{D_s}} <$ 20 GeV/$c$, a kaon momentum $p_{\mathrm{K}} > 1.5$ GeV/$c$, a pion momentum $p_\pi > 1$ GeV/$c$, a fitted decay length $\delta\ell > 500$ $\mu$m, and a photon energy $E_\gamma < 3$ GeV. The $\mathrm{b\bar{b}}$ purity of this $\mathrm{D_s^{*+}}$ signal is 85%. In the other subsample, enriched in $\mathrm{c\bar{c}}$ events, the requirements are $p_{\mathrm{D_s}} > 20$ GeV/$c$, $p_{\mathrm{K}} > 2.5$ GeV/$c$, $p_\pi > 1.5$ GeV/$c$, $\delta\ell > 0$, and $E_\gamma < 5$ GeV, corresponding to a purity of the $\mathrm{D_s^{*+}}$ signal of about 60% in $\mathrm{c\bar{c}}$ events. In Fig. 5 the $M(\mathrm{D_s^*}) - M(\mathrm{D_s})$ distributions with calorimetric photons and conversions are plotted.

## 3.6 $\Lambda_c^+$ Baryon

The $\Lambda_c^+$ is observed via the decay mode $\Lambda_c^+ \to \mathrm{pK^-\pi^+}$. To form a $\Lambda_c^+$ candidate three tracks are required, each having at least one vertex detector hit. The momenta must be greater than 5.0 GeV/$c$, 3.0 GeV/$c$ and 1.0 GeV/$c$ for the proton, kaon and pion candidates respectively and the total energy must exceed $0.2 \times E_{\mathrm{beam}}$. For particle identification, $|\chi_h| < 2.5$ is required for the given particle hypothesis and two pion veto cuts are applied: $\chi_\pi < -2.0$ for the proton candidate and $\chi_\pi < -1.0$ for the kaon candidate.

After a $\chi^2$ fit of the tracks to a common vertex the $\chi^2$ probability has to be greater than 1%. The mass distribution of the $\Lambda_c^+$ candidates is shown in Fig. 6.

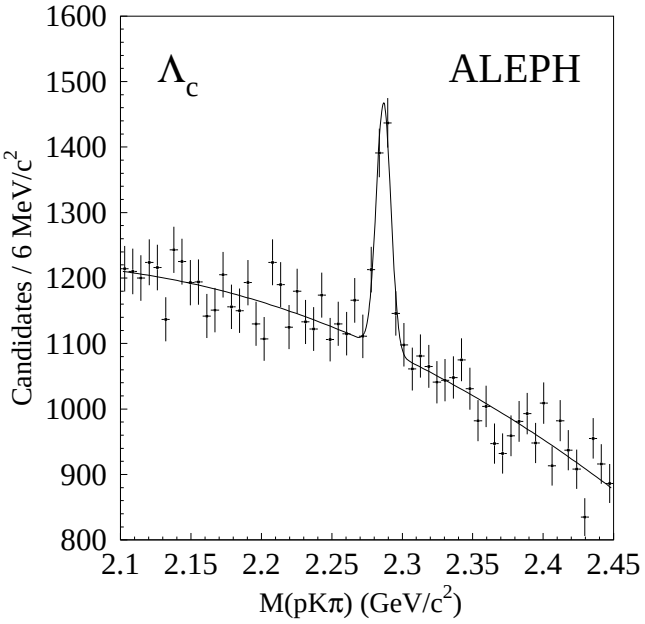


Figure 6: $\mathrm{pK^-\pi^+}$ invariant mass distribution with the fit result.

# 4 $D^{*+}$ Spectrum and Charm Fragmentation

Because of its large signal/background ratio, the $D^{*+}$ sample, selected as described in section 3.2, is used to measure the fractional energy spectrum. The $X_E$ range between 0.1 and 1.0 is divided into 18 equal bins. In each bin, an analytical form is fitted outside the $D^{*+}$ peak to the mass-difference distribution, so that the background can be subtracted bin by bin. The efficiency-corrected $X_E$ distribution is shown in Fig. 7 and the numerical values of the production rates are given in Table 1.

Table 1: Differential $D^{*\pm}$ production rate as a function of the fractional energy $X_E$. The errors are statistical only.

| $X_E$ range | $1/N(Z\to\text{hadrons})\times(dN(D^{*\pm})/dX_E)$ $(10^{-3})$ |
|---|---|
| 0.10-0.15 | $7.47 \pm 0.63$ |
| 0.15-0.20 | $9.03 \pm 0.49$ |
| 0.20-0.25 | $10.42 \pm 0.44$ |
| 0.25-0.30 | $10.76 \pm 0.43$ |
| 0.30-0.35 | $9.89 \pm 0.38$ |
| 0.35-0.40 | $8.97 \pm 0.35$ |
| 0.40-0.45 | $8.17 \pm 0.32$ |
| 0.45-0.50 | $6.94 \pm 0.28$ |
| 0.50-0.55 | $6.73 \pm 0.27$ |
| 0.55-0.60 | $5.56 \pm 0.24$ |
| 0.60-0.65 | $4.94 \pm 0.22$ |
| 0.65-0.70 | $3.49 \pm 0.18$ |
| 0.70-0.75 | $3.13 \pm 0.17$ |
| 0.75-0.80 | $2.00 \pm 0.14$ |
| 0.80-0.85 | $1.27 \pm 0.11$ |
| 0.85-0.90 | $0.50 \pm 0.07$ |
| 0.90-0.95 | $0.27 \pm 0.05$ |
| 0.95-1.00 | $0.06 \pm 0.03$ |

The $D^{*+}$ spectrum is interpreted as the sum of three contributions: hadronisation of a charm quark produced in a $Z \to c\bar{c}$ decay, decay of a bottom hadron from a $Z \to b\bar{b}$ decay, and gluon splitting into a pair of heavy quarks which hadronise or decay into a $D^{*+}$. The $X_E$ distribution of the three contributions are taken from the Monte Carlo simulation which uses the Peterson *et al.* fragmentation scheme [9] for heavy quarks. The $b\bar{b}$ contribution is compared with data using a high purity b-tag in the opposite hemisphere (Fig. 8). A possible contamination from two-photon production has been investigated by a Monte Carlo study normalised to data [10] and found to be negligible ($< 0.25\%$).

To describe the production mechanism, three parameters are fitted to the data : the fraction $f_g$ of $D^{*+}$ from gluon splitting, the fraction $f_b$ of $b\bar{b}$ events in the remaining (no gluon splitting) sample, and the Peterson fragmentation parameter $\varepsilon_c$. The fit is carried out in two steps iteratively. Firstly a two-dimensional fit to the distribution ($X_E$,$\mathcal{B}_{\text{tag}}$), where $\mathcal{B}_{\text{tag}}$ is the tagging variable described in Section 2 is performed in order to constrain $f_b$. $X_E$ is required to be larger than 0.25 to reduce to a negligible

level the gluon splitting contribution. The shape of the c and b contributions are taken from a full Monte Carlo simulation. The small gluon splitting contribution is taken in size and shape from the Monte Carlo simulation. The combinatorial background distribution is taken from the side band of the $\mathrm{K}\pi\pi - \mathrm{K}\pi$ mass difference in the data sample. The ($X_E$,$\mathcal{B}_{\mathrm{tag}}$) plane is segmented into 62 bins of variable size in such a way that they all contain enough statistics for a $\chi^2$ fit of $f_{\mathrm{b}}$ to be performed.

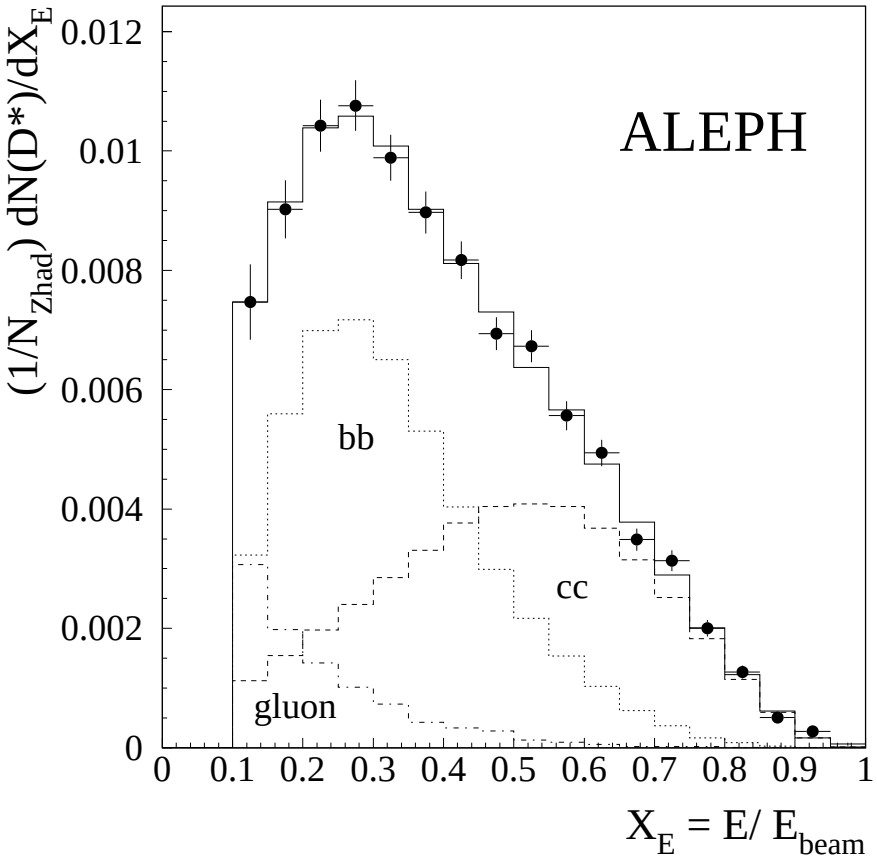


Figure 7: Distribution of $X_E$ for the $\mathrm{D}^{*\pm}$'s. The data (points with error bars) are compared to the fit described in the text. The three contributions: $\mathrm{b\bar{b}}$ (dotted line), $\mathrm{c\bar{c}}$ (dashed line) and gluon splitting to heavy quarks (dashed-dotted) are shown.

In a second step, fixing $f_{\mathrm{b}}$ to this value, $f_{\mathrm{g}}$ and $\varepsilon_{\mathrm{c}}$ are extracted from a fit to the $X_E$ distribution using the function

$$(1-f_{\mathrm{g}})\left[f_{\mathrm{b}}\frac{1}{N_{\mathrm{b\bar{b}}}}\frac{dN^{\mathrm{b\bar{b}}}}{dX_E}+(1-f_{\mathrm{b}})\frac{1}{N_{\mathrm{c\bar{c}}}}\frac{dN^{\mathrm{c\bar{c}}}}{dX_E}\right]+f_{\mathrm{g}}\frac{1}{N_{\mathrm{g}\to\mathrm{c\bar{c}}}}\frac{dN^{\mathrm{g}\to\mathrm{c\bar{c}}}}{dX_E}. \qquad (1)$$

The two steps are iterated and once convergence is reached, a minimal $\chi^2$ of the 2D fit of 71.3 for 61 degrees of freedom is obtained for $f_b = 0.534 \pm 0.016$, corresponding to $R_b\ f(b \to \mathrm{D}^{*\pm})/R_c\ f(c \to \mathrm{D}^{*+}) = 1.15 \pm 0.06$. The uncertainty of this measurement is statistically dominated. The fitted distribution of the $\mathcal{B}_{\mathrm{tag}}$ variable is shown in Fig. 9, compared with data.

The result of the 1D-fit is shown in Fig. 7; it has a $\chi^2$ of 11.9 for 14 degrees of freedom (the last three bins are grouped together in the fit). The fitted value of $f_{\mathrm{g}}$ is

related to the average number of gluon splitting events to charm per Z hadronic decay and gives $\bar{n}_{g\to c\bar{c}} = (4.7 \pm 1.0(\text{stat.}))\%$. The systematic error on this result however is large, due to the efficiency uncertainties at low $X_E$. In the fit, the JETSET [8] Monte Carlo shape for the gluon splitting and the Peterson parameterisation for the heavy quark fragmentation functions [9] are assumed. In the next section, a more sensitive analysis dedicated to this measurement is described.

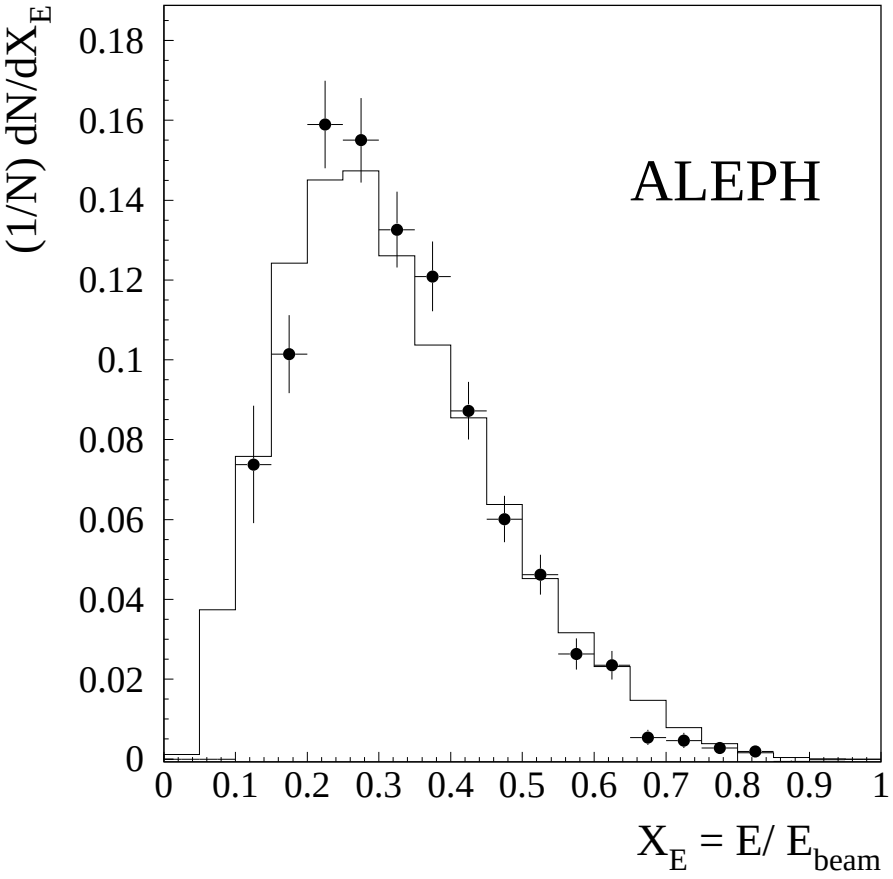


Figure 8: Distribution of $X_E$ for the $D^{*+}$'s from the $b\bar{b}$ source compared with the Monte Carlo prediction. The data (points with error bars) are obtained by applying the lifetime-mass btag on the hemisphere opposite to the $D^{*\pm}$, and corrected for efficiency. The remaining charm contribution is subtracted.

The fitted value $\varepsilon_c = (33.9 \pm 3.7) \times 10^{-3}$ can be converted into a measurement of the average fractional energy of the $D^{*+}$ in $Z \to c\bar{c}$ events of

$$\langle X_E(D^*)\rangle_{c\bar{c}} = 0.4878 \pm 0.0046(\text{stat.}) \pm 0.0061(\text{syst.}).$$

The quoted systematic uncertainty is dominated by the choice of parameterisation of the fragmentation function, as in Ref. [1].

Using the Monte Carlo shape for the very small extrapolation to the entire $X_E$ range (from 0.1 to the threshold at 0.044), the number of $D^{*\pm}$ per hadronic Z decay in the mode considered is found to be

$$\bar{n}_{D^{*\pm}} \times B(D^{*+} \to D^0\pi^+) \times B(D^0 \to K^-\pi^+) = (5.114 \pm 0.067(\text{stat.}) \pm 0.072(\text{syst.})) \times 10^{-3}.$$

A 0.5% uncertainty from the finite Monte Carlo statistics is included in the statistical uncertainty. This result includes the gluon splitting contribution. Subtracting this contribution and using the ratio of the $b\bar{b}$ to the $c\bar{c}$ contribution quoted above, the probability for a c-quark to hadronise into a $D^{*+}$ is measured to be

$$f(c \to D^{*+}) = 0.2333 \pm 0.0102(\text{stat.}) \pm 0.0084(\text{syst.}) \pm 0.0074(\text{B.R.}).$$

The normalisation of this result relies on the branching fraction given in ref. [14].

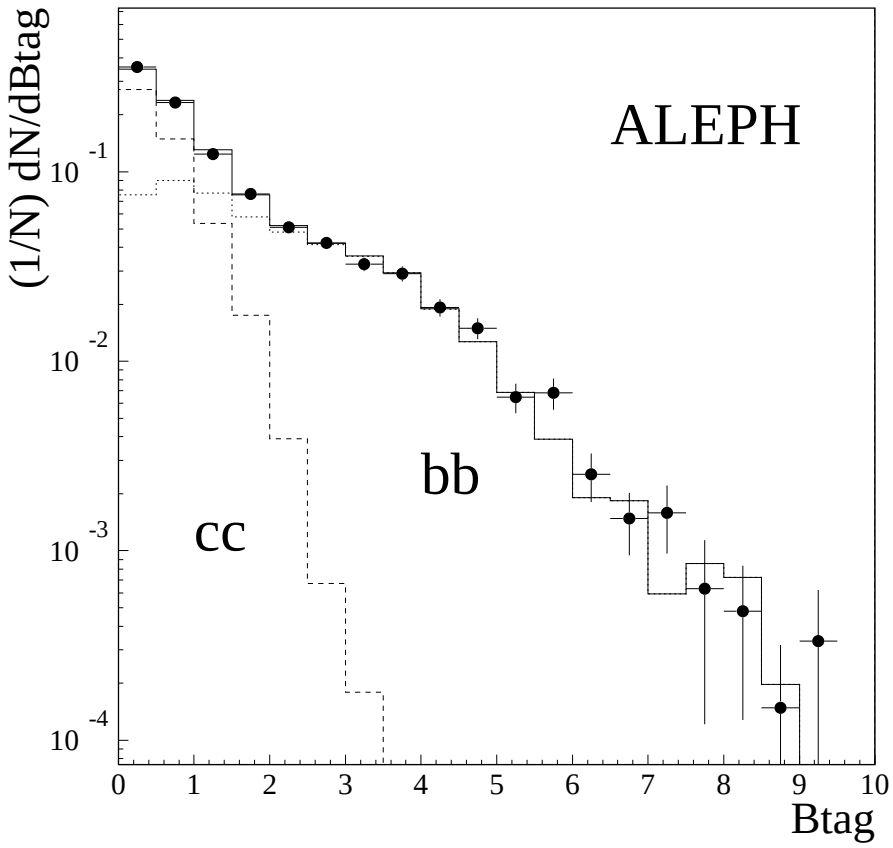


Figure 9: Distribution of the b-tagging variable for the $D^{*\pm}$'s with $X_E > 0.25$ The data (points with error bars) are compared with the projection onto the $\mathcal{B}_{tag}$ axis of the fit described in the text. The two contributions: $b\bar{b}$ (dotted line) and $c\bar{c}$ (dashed line) are shown.

Systematic errors on these quantities arise from various sources. The uncertainty from $f_b$ has been evaluated by varying it by $\pm 1$ standard deviation. The uncertainty on the efficiency has been estimated on a cut by cut basis. The uncertainty from the mass and mass-difference cuts have been assessed by varying the fitted mass and mass difference within errors yielding a 0.5% and 0.3% contribution to the relative error on the efficiency. The Prob($\chi^2$) cut efficiency has been compared between data at high $X_E$ and Monte Carlo, and found to differ by 8.3%. This is taken as the uncertainty on the efficiency of this cut and results in a 0.6% uncertainty on the overall normalisation. To assess the uncertainty from the cut on decay length significance, the resolution on this quantity has been varied by 10%. The resulting relative change in efficiency is

found to be $(1.6 \pm 0.6)\%$ for the $\delta\ell/\sigma > 0$ cut and $(0.06 \pm 0.90)\%$ for the $\delta\ell/\sigma > 1$ cut. Taking a 1.6% uncertainty in the range $0.3 < X_E < 0.4$ and 0.9% for $X_E$ below 0.3, the resulting uncertainty on the overall normalisation is 0.4%. The probability of nuclear interaction in the detector is simulated at the 10% level, determined from a study of tau pairs where the pion from one of the taus undergoes such an interaction in the detector. This yields a 0.7% relative error on the efficiency. For the systematics from background subtraction, the analytical shape of the background has been modified and the fit range for the mass-difference fit has been varied. This results in a 0.2% overall error on the absolute normalisation, localised in the first three $X_E$ bins where the background is large (the uncertainty reaches 4.5% in the first bin). Summing linearly the errors from the $P(\chi^2)$ cut and the $\delta\ell/\sigma$ cut, as they both pertain to vertexing and are strongly correlated, and then summing in quadrature all the contributions, the overall normalisation uncertainty is 1.4%. Details are given in Table 2. As a check, the whole analysis has been repeated with the decay length significance cut relaxed by 1 unit and the cut in $\chi^2$ probability for the $D^0$ vertex removed. The final number of events changes by 1%.

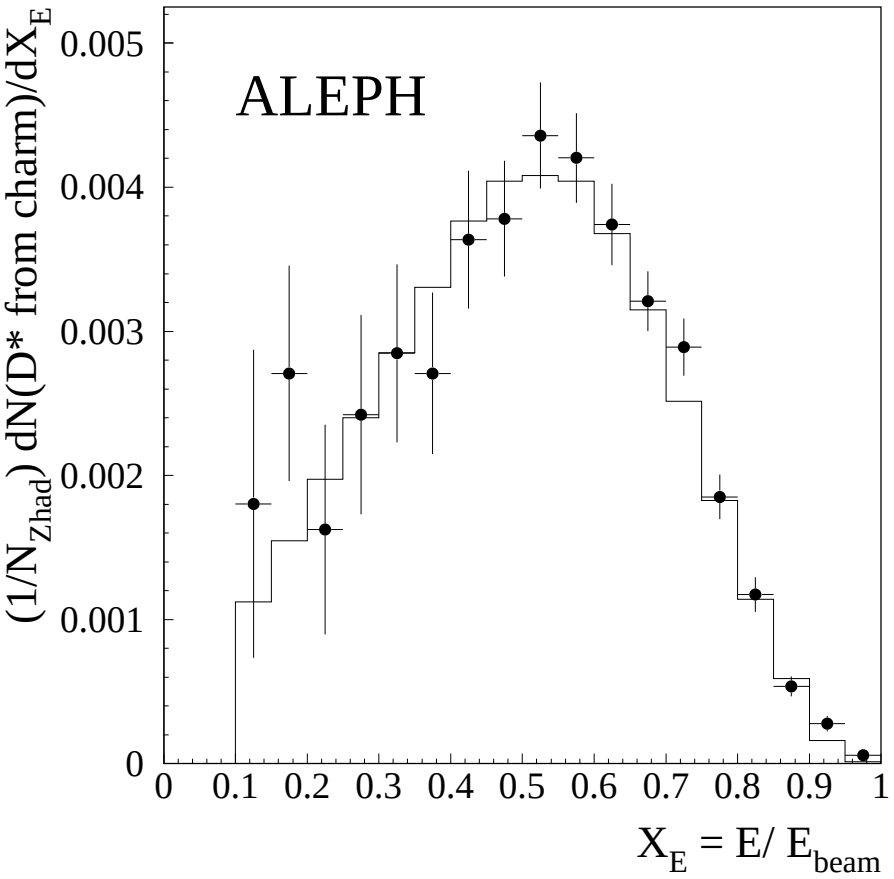


Figure 10: Distribution of $X_E$ for the $D^{*\pm}$'s from the $c\bar{c}$ source. The data (points with error bars) are compared to the Monte Carlo simulation.

Some of these systematic effects are $X_E$ dependent. They have been propagated to the gluon splitting measurement and the average $X_E$ measurement.

As a check on the stability of the result, the fit has been repeated with $f_b$ left free. The fitted parameters are perfectly consistent with the result of the whole procedure,

but the uncertainty on $f_b$ is increased by a factor of 1.7.

In Fig. 10, the spectrum of the D*s from charm is shown. This spectrum (points with error bars) is obtained from the data points of Fig. 7 or Table 1, from which the b contribution and the gluon splitting contribution are subtracted. The b contribution is extracted from the b-tagged data of Fig. 8, normalised using the fitted $f_{\rm b}$. The Monte Carlo shape, normalised to the measurement presented in the next section, is used for the gluon-splitting contribution.

Table 2: Relative systematic errors in percent on the $\rm D^{*\pm}$ production rate measurement. Some of them are strongly $X_E$ dependent (see text). The two vertexing uncertainties are considered as fully correlated and added linearly.

| Source | $\delta\epsilon/\epsilon$ |
|---|---|
| $\Delta M$ cut | 0.3% |
| $M(\rm K\pi)$ cut | 0.5% |
| $\rm P(\chi^2)$ cut | 0.6% |
| $\delta\ell/\sigma$ cut | 0.4% |
| nuclear interactions | 0.7% |
| Backg. subtraction | $\delta N/N = 0.2\%$. |
| Total systematics | 1.4% |

# 5 Measurement of the Gluon Splitting Rate to $\rm c\bar{c}$

In order to determine more precisely the rate $\bar{n}_{\rm g\to c\bar{c}}$ one more variable, related to the event topology, has been used. In a $\rm g \to c\bar{c}$ event the two quarks from the gluon splitting, together with one of the primary quarks, tend to end up in the same hemisphere, resulting in a large invariant mass for this hemisphere and a relatively light opposite hemisphere. Denoting by $M_{\rm heavy}$ ($M_{\rm light}$) the invariant mass of the heavier (lighter) hemisphere in an event, the difference $\Delta M_H = M_{\rm heavy} - M_{\rm light}$ has been used to discriminate between D*'s produced from primary quarks and from gluons. The distributions of $\Delta M_H$, as given by the JETSET event generator [8], are shown in Fig. 11. In JETSET D*'s from primary quarks are nearly evenly shared among the hemispheres while $\approx 75\%$ of the D*'s from gluons are found in the heavy hemisphere.

The sample of reconstructed $\rm D^{*+}$ mesons is divided into two samples depending upon whether the $\rm D^{*+}$ is in the light or heavy hemisphere. A two–dimensional binned likelihood fit is then performed to the distributions in the $X_E/\Delta M_H$ plane of these two samples using the function :

$$(1-f_{\rm g})\left[f_{\rm b}\frac{1}{N_{\rm b\bar{b}}}\frac{d^2N^{\rm b\bar{b}}}{dX_E d\Delta M_H} + (1-f_{\rm b})\frac{1}{N_{\rm c\bar{c}}}\frac{d^2N^{\rm c\bar{c}}}{dX_E d\Delta M_H}\right] + f_{\rm g}\frac{1}{N_{\rm g\to c\bar{c}}}\frac{d^2N^{\rm g\to c\bar{c}}}{dX_E d\Delta M_H}. \quad (2)$$

For this analysis the event selection has been tightened in order to ensure that the event is fully contained in the detector: The total energy $E_{\rm ch}$ of all charged tracks

is required to exceed 15 GeV and events strongly unbalanced in momentum projected along the beam axis $p_z$ are rejected by requiring $|\sum p_z|/E_{\rm ch} < 40\%$. This selection has an efficiency of 89.3% for hadronic Z decays without the process $g \to Q\bar{Q}$ and 91.9% for $g \to Q\bar{Q}$ events (Q stands for b or c), as estimated from Monte Carlo.

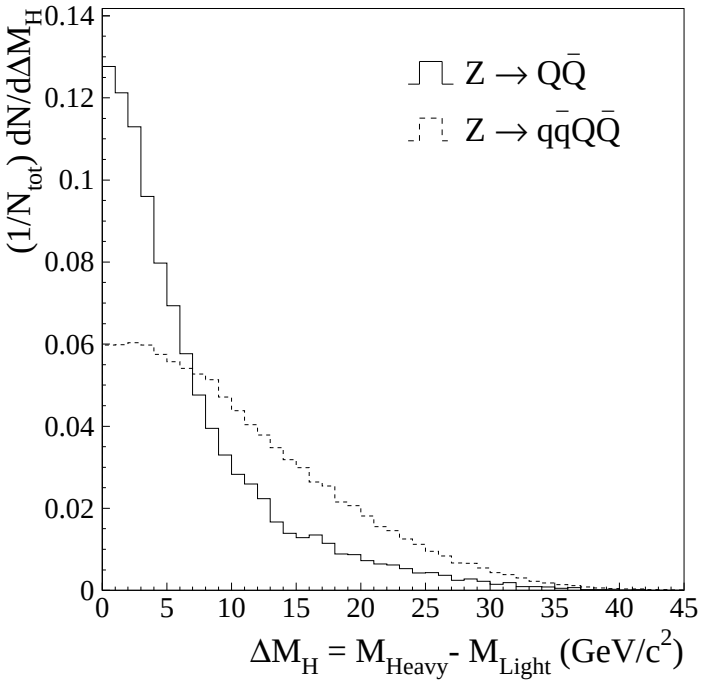


Figure 11: Difference of heavy and light hemisphere masses in Z decays with (dashed line) and without (full line) gluon splitting to heavy quarks (from JETSET). The events entering these distributions are required to contain at least one $D^{*\pm}$. Q stands for b and c, and q for all flavours.

The $D^{*+}$ mesons are reconstructed with cuts similar to the ones used in section 3. The hemispheres are defined by a plane perpendicular to the thrust axis and their invariant masses are calculated using energy flow objects with an energy above 1 GeV. Again, the analysis proceeds in two steps. A fit to the one–dimensional $\mathcal{B}_{\rm tag}$ distribution yields the fraction $f_{\mathcal{B}tag} = 0.524 \pm 0.015$ of $D^*$ from b hadron decays in the selected sample. The error includes the systematic uncertainties but is dominated by the statistical error. Then the two two-dimensional distributions $X_E/\Delta M_H$, depending upon whether the $D^*$ is in the heavy or light hemisphere, are fitted simultaneously using a binned likelihood fit ($18\times18$ bins). The b-contribution excluding gluon splitting $f_{\rm b}(1-f_{\rm g})$ is constrained to $f_{\mathcal{B}tag}$ by a $\chi^2$ term. The result of the fit is

$$f_{\rm g} = 0.0522 \pm 0.0077\,,\ f_{\rm b} = 0.5308 \pm 0.0098$$

from which $\bar{n}_{g\to c\bar{c}}$ is computed as

$$\bar{n}_{g\to c\bar{c}} = R_{\rm c}\frac{\epsilon_{\rm c}}{\epsilon_{g\to c\bar{c}}}\frac{1}{1-f_{\rm b}}\left[\frac{f_{\rm g}}{1-f_{\rm g}} - \frac{1}{R_{\rm b}}\frac{\epsilon_{g\to b\bar{b}}}{\epsilon_{\rm b}} f_{\rm b}\bar{n}_{g\to b\bar{b}}\right] \quad (3)$$

$$= (3.23 \pm 0.48({\rm stat.}))\%\ . \quad (4)$$

Here, $\epsilon_i$ is the efficiency to reconstruct a $D^{*+}$ from a given source $i$. The term in brackets provides a $\sim 10\%$ correction for the $g \to b\bar{b}$ contribution which is taken from ref. [11]:

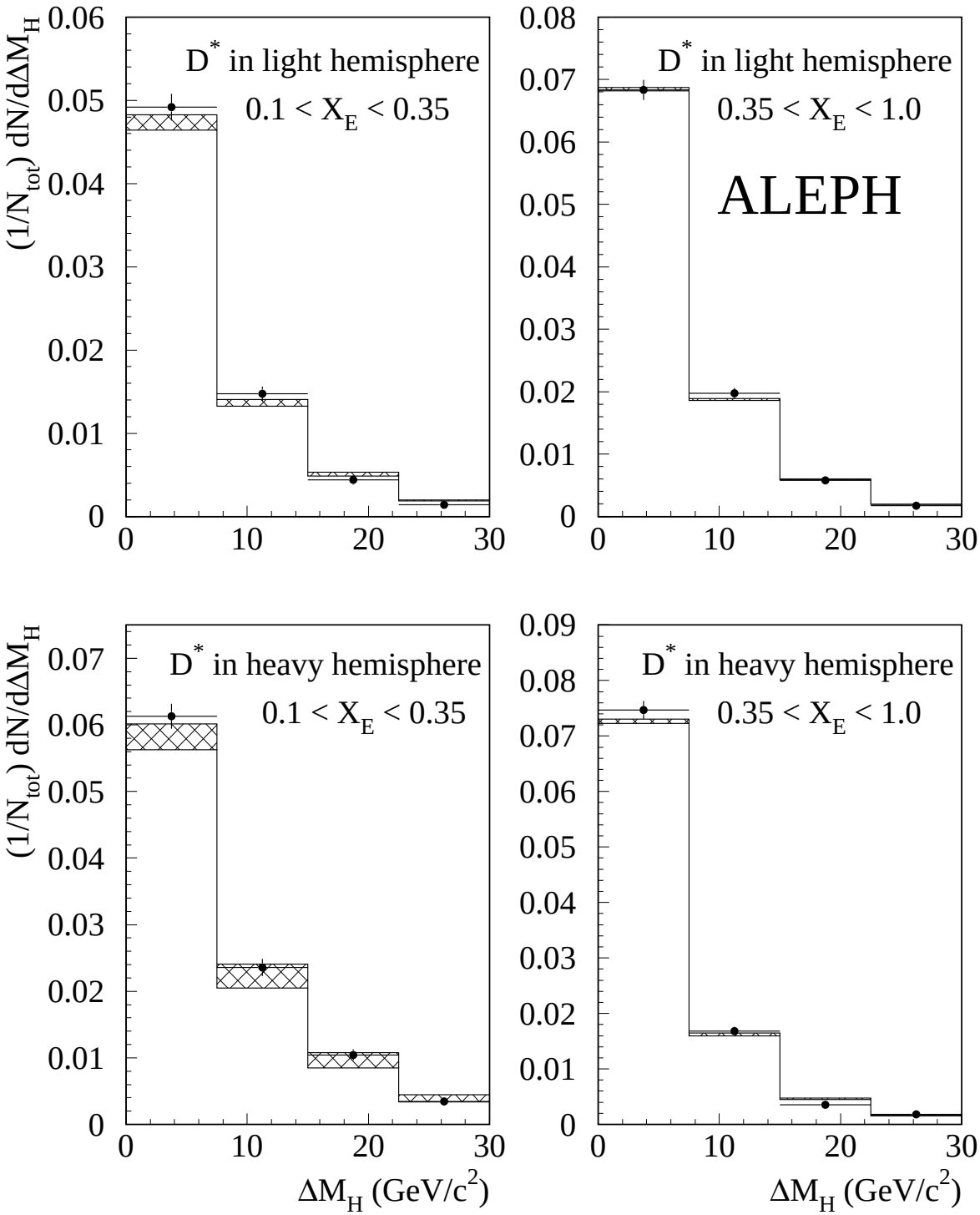


Figure 12: Hemisphere mass difference distributions. The data (points) are subdivided into four bins with $D^*$ in the heavy/light hemisphere and for low/high $X_E$. The fitted contribution from primary quarks is shown as the solid histogram, the $g \to Q\bar{Q}$ contribution is added as cross-hatched area.

$\bar{n}_{g\to b\bar{b}} = (2.77 \pm 0.42 \pm 0.57) \times 10^{-3}$. In Fig. 12 projections of the two-dimensional distributions on $\Delta M_H$ are shown for the two hemispheres for two ranges in $X_E$. The agreement between data and Monte Carlo is good, in particular it can be seen that the high-$X_E$ data are well described without the gluon splitting contribution but that its inclusion is necessary for $X_E < 0.35$ in the heavy hemisphere. The $\chi^2$ probability for this distribution degrades from 0.40 to 0.001 for the four bins when the gluon splitting contribution is neglected. In order to show more clearly the shape of the gluon splitting signal in this region, Fig .13 shows the data with the fitted contribution from primary quarks subtracted. Good agreement with the Monte Carlo prediction is observed.

Systematic errors have been studied for the efficiency of $D^*$ reconstruction, the fitting procedure, the modelling of the Monte Carlo distributions, and the parameters entering Eq. (3). They are summarised in Table 3.

The errors on the number of reconstructed $D^{*+}$'s have been estimated as in the

Table 3: List of absolute systematic errors on $\bar{n}_{g\to c\bar{c}}$

| Source | $\Delta\bar{n}_{g\to c\bar{c}}$ $(10^{-2})$ |
|---|---|
| $D^{*\pm}$ reconstruction | 0.25 |
| Monte Carlo statistics | 0.19 |
| b–contribution | 0.09 |
| Hemisphere selection | 0.15 |
| $\varepsilon_c$ | 0.15 |
| $\varepsilon_b$ | 0.19 |
| $X_E(b \to D^*)$ from data | 0.15 |
| $D^{**} \to D^* X$ | 0.04 |
| $\Lambda_{PS}$ | 0.15 |
| Hard gluon | 0.08 |
| HERWIG | 0.11 |
| ARIADNE | 0.21 |
| Total | 0.53 |

previous section by comparing the efficiencies of the cuts between Monte Carlo and data and varying them within their uncertainties. The normalization of the background has also been changed within the errors.

The finite Monte Carlo statistics has been accounted for by repeating the fit with the distributions randomly smeared. The fit has also been redone not applying the $\chi^2$ constraint on the b contribution, and leaving free the relative fractions of $D^*$'s in the two hemispheres for the c and b contributions separately.

Several parameters affecting the shape of the Monte Carlo distributions have been varied: $\varepsilon_c$ has been changed within the errors derived from the above measurement and $\varepsilon_b$ within $\varepsilon_b = 0.0045 \pm 0.0009$. The $X_E$ shape for $b \to D^*$ as derived from the b–tagged sample has been used for the fit. The dependence of the fraction of $D^*$ mesons originating from a $D^{**}$ has been estimated by changing this rate by $\pm 30\%$ for b and c separately.

The effects of gluon emission in the parton shower have been assessed by changing the JETSET parameter $\Lambda_{PS}$ such that it corresponds to a $\pm 4\%$ variation in $\alpha_s(M_Z)$. The rate of events in which both primary quarks recoil against a hard gluon and populate the same hemisphere has been varied by 30%. Finally, the $\Delta M_H$ shapes as

given by HERWIG 5.8 [12] and ARIADNE 4.08 [13] have been used. For ARIADNE, the transverse momentum of a splitting gluon was required to be larger than its virtuality, as suggested in Ref. [16]. ARIADNE yields the largest discrepancy and this has been taken as the systematic error on the Monte Carlo model. Adding all systematic errors quadratically, the average fraction of hadronic Z decays where a gluon splits in a $c\bar{c}$ pair is found to be

$$\bar{n}_{g\to c\bar{c}} = (3.23 \pm 0.48(\text{stat.}) \pm 0.53(\text{syst.}))\% \ .$$

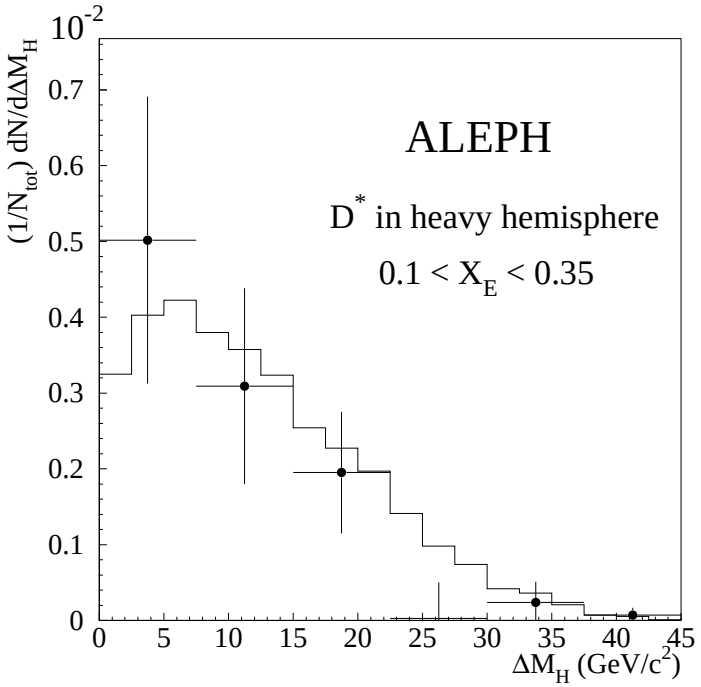


Figure 13: Comparison of the data with the fitted contribution from primary quarks subtracted (points) and the predicted gluon splitting distribution (histogram).

# 6 Measurement of the $D_s^{*\pm}$ production rate

The selection efficiencies for finding $D_s^{*\pm}$ mesons are evaluated from the Monte Carlo using the mix of $D_s^{\pm} \longrightarrow \phi\pi^{\pm}$ and $D_s^{*+} \longrightarrow \bar{K}^{*0}K^{+}$ decays predicted by the branching ratios in [14]. They are given in Table 4 for the selection described in Section 3.5.

Table 4: Selection efficiencies for $D_s^{*\pm}$ mesons (the errors are statistical only).

| | conversions | | calorimetric photons | |
|---|---|---|---|---|
| | $Z \to c\bar{c}$ (%) | $Z \to b\bar{b}$ (%) | $Z \to c\bar{c}$ (%) | $Z \to b\bar{b}$ (%) |
| $c\bar{c}$-enriched | $0.38 \pm 0.04$ | $0.12 \pm 0.02$ | $2.72 \pm 0.12$ | $0.85 \pm 0.07$ |
| bb-enriched | $0.10 \pm 0.02$ | $0.29 \pm 0.03$ | $0.57 \pm 0.05$ | $1.60 \pm 0.09$ |

The number of events in the data samples was evaluated by fitting the $D_s^{*+}$ spectrum with the sum of two Gaussian functions for the signal and a polynomial for the

background. In the case of the calorimetric photons, the means and widths of the two Gaussians and the ratio of their area are taken from Monte Carlo. For converted photons the means of the two Gaussians and the width of the broad one are left free in the fit. The background is parameterised to reproduce the Monte Carlo. From the fit the number of events in the $c\bar{c}$-enriched sample is $N_c = 26 \pm 7$ $(139 \pm 22)$ and in the $b\bar{b}$-enriched is $N_b = 36 \pm 11$ $(106 \pm 37)$ with converted (calorimetric) photons. The production rates $f(c \to \mathrm{D_s^{*\pm}})$ and $f(b \to \mathrm{D_s^{*\pm}})$ can be calculated by solving two equations of the following form, corresponding to the $\mathrm{c\bar{c}}$ and $\mathrm{b\bar{b}}$ enriched samples:

$$\begin{aligned} N_{\mathrm{D_s^{*+}}} &= 2N_{\mathrm{q\bar{q}}} \times B(\mathrm{D_s^{*+}} \to \mathrm{D_s^+}\gamma) B(\mathrm{D_s^+} \to \phi\pi^+) B(\phi \to \mathrm{K^+K^-}) \\ &\quad \times [\mathrm{R_c} f(\mathrm{c} \to \mathrm{D_s^{*+}}) \epsilon_\mathrm{c} + \mathrm{R_b} f(\mathrm{b} \to \mathrm{D_s^{*\pm}}) \epsilon_\mathrm{b}], \end{aligned} \tag{5}$$

where $N_{\mathrm{q\bar{q}}}$ is the number of hadronic events in the data sample, $\epsilon_\mathrm{c}$ ($\epsilon_\mathrm{b}$) the selection efficiency for $\mathrm{D_s^*}$ mesons in $\mathrm{c\bar{c}}$ ($\mathrm{b\bar{b}}$) events and $f(\mathrm{c} \to \mathrm{D_s^*})$ ($f(\mathrm{b} \to \mathrm{D_s^*})$) the probabilities of a c (b) quark giving rise to a $\mathrm{D_s^*}$ meson. A similar formula can be written for the $\mathrm{D_s^+} \longrightarrow \mathrm{K^{*0}K^+}$ channel. The results from the whole data sample are:

$$\begin{aligned} f(\mathrm{c} \to \mathrm{D_s^{*+}}) &= 6.9 \pm 1.8 \text{ (stat.)} \pm 0.7 \text{ (syst.)} \pm 1.8(\mathrm{BR})\% \\ f(\mathrm{b} \to \mathrm{D_s^{*+}}) &= 11.3 \pm 3.5 \text{ (stat.)} \pm 1.0 \text{ (syst.)} \pm 2.8(\mathrm{BR})\% \end{aligned}$$

Here the last error is due to the final state branching ratios taken from [14], while the systematic error includes the uncertainty in the selection efficiencies and background parameterisation in the fit. The latter contribution is evaluated using different functional shapes for the background; a further check is made by taking the background shape evaluated bin by bin from Monte Carlo and using it in the fit.

# 7 Production Rates of the Ground States

## 7.1 Production of $\mathrm{D^0}$ and $\mathrm{D^+}$

The number of $\mathrm{D^0}$ and $\mathrm{D^+}$ present in the samples are extracted from a fit to the invariant mass distributions (Figs 1, 3), where the signal is parameterised by two gaussians with a common mean and the combinatorial background by a polynomial function. Resonant background contributions, such as $\mathrm{D^0} \to \mathrm{K^-K^+}$, $\mathrm{D_s^+} \to \phi\pi^+$, $\mathrm{D_s^+} \to \bar{\mathrm{K}}^*\mathrm{K}$, and $\mathrm{D^0} \to \mathrm{K^-}\pi^+$ where the two mass assignments are reversed, are taken into account in the fit. The fractions of $\mathrm{D^0}$ and $\mathrm{D^+}$ originating from the process $\mathrm{Z} \to \mathrm{c\bar{c}}$ are measured by applying, on the hemisphere opposite to the reconstructed D meson, the lifetime-mass tag [5] selecting b hemispheres with 99% purity. The charm fraction in the D meson samples is then given by $f_\mathrm{c} = \frac{\epsilon_{\mathrm{Bb}} - r_{\mathrm{b}-tag}}{\epsilon_{\mathrm{Bb}} - \epsilon_{\mathrm{Bc}}}$ where $r_{\mathrm{b}-tag}$ is the fraction of D mesons surviving the b-tag cut. The b hemisphere b-tag efficiency $\epsilon_{\mathrm{Bb}}$ is evaluated on data using a double-tag technique and $\epsilon_{\mathrm{Bc}}$, the c hemisphere b-tag efficiency, is obtained from Monte Carlo simulation [5]. Both efficiencies are corrected for the selection bias induced by requiring the presence of a high momentum D meson in the opposite hemisphere. The fractions of $\mathrm{D^0}$ and $\mathrm{D^+}$ mesons from charm are found to be: $f_\mathrm{c}(\mathrm{D^0}) = 0.787 \pm 0.019$ ; $f_\mathrm{c}(\mathrm{D^+}) = 0.797 \pm 0.020$, where the quoted errors are statistical.

The small fraction of D mesons from gluon splitting has been deduced using the measurement from section 5, the ALEPH measurement $\bar{n}_{\mathrm{g} \to \mathrm{b\bar{b}}} = (2.77 \pm 0.42 \pm 0.57) \times$

$10^{-3}$ [11], and the efficiency ratio for the selection of a D meson $\frac{\epsilon_{g\to D}}{\epsilon_{q\to D}}$ obtained from simulation.

The number of fitted D mesons, together with the charm fractions and the gluon splitting contamination, are reported in Table 5.

Table 5: $D^0$ and $D^+$ selection: number of candidates; fraction of $c \to D$ mesons in the sample; efficiency of $c \to D$ meson reconstruction; percentage of D mesons from gluon splitting. All quoted errors are statistical.

| | N. candidates | Charm fraction | Efficiency | $g\to Q\bar{Q}(\%)$ |
|---|---|---|---|---|
| $D^0$ | $7871 \pm 129$ | $0.787 \pm 0.019$ | $0.200 \pm 0.004$ | 0.8 |
| $D^+$ | $7409 \pm 153$ | $0.797 \pm 0.020$ | $0.191 \pm 0.002$ | 0.8 |

From the numbers in Table 5, the following branching fractions are obtained:

$$R_c \times f(c \to D^0) \times B(D^0 \to K^-\pi^+) = (0.370 \pm 0.011) \times 10^{-2}$$

$$R_c \times f(c \to D^+) \times B(D^+ \to K^-\pi^+\pi^+) = (0.368 \pm 0.012) \times 10^{-2}$$

Different sources of systematic uncertainty have been investigated and are given in Table 6. The first three errors are related to the detector performance. The fraction of

Table 6: Relative systematic errors in percent on the $D^0$, $D^+$, $D_s^+$ and $\Lambda_c^+$ production rate measurements.

| Source | $D^0$ (%) | $D^+$ (%) | $D_s^+$ (%) | $\Lambda_c^+$ (%) |
|---|---|---|---|---|
| Nuclear interact. | 0.5 | 0.7 | 0.3 | 0.3 |
| $dE/dx$ | 0.9 | 0.4 | 1.2 | 2.2 |
| vertexing | 3.8 | 2.3 | 1.7 | 1.7 |
| charm fraction | 0.7 | 0.7 | - | - |
| gluon splitting | 0.3 | 0.3 | 0.3 | 0.3 |
| fragmentation | 3.7 | 3.7 | 1.9 | 4.0 |
| charm physics | 1.6 | 2.1 | - | - |
| fitting funct. | 1.5 | 1.5 | 4.0 | 1.6 |
| MC stat. | 2.0 | 1.0 | 3.0 | 2.0 |
| Total systematics | 6.2 | 5.3 | 5.8 | 5.5 |

tracks with $dE/dx$ information has been compared between data and Monte Carlo with a sample of candidates selected in the side-band regions of the $D^0$ and $D^+$. The Monte Carlo has been corrected for differences and the uncertainty on the ratio data/MC has been taken as a systematic error. The $dE/dx$ calibration and resolution have been studied on data for a pure kaon sample from the decay mode $D^{*+} \to D^0\pi^+$, $D^0 \to K^-\pi^+$. Data/MC differences have been taken into account to obtain the $dE/dx$ cut efficiency and the associated systematic error. The fraction of D mesons forming a common vertex with a $\chi^2$-probability greater than 1% is obtained from data, from the fraction of selected candidates under the D meson mass peak, corrected by the fraction of

background candidates estimated on sideband regions. The resolution on the decay-length measurement has been checked on $D^0$ and $D^+$ sideband samples, where most of the candidates carry no lifetime information. The difference found between data and Monte Carlo has been taken as a systematic error for the decay length significance cut together with the error coming from the $D^0$ and $D^+$ lifetime uncertainties. The fraction of tracks not reconstructed due to nuclear interaction in the $D^0 \to K^-\pi^+$ and $D^+ \to K^-\pi^+\pi^+$ decays is estimated from Monte Carlo to be 5 % and 7 % respectively, with a systematic error of 10 %.

The main systematic error on the determination of the charm fraction comes from the correction factor applied to the b-tag efficiencies. This arises from the selection of an energetic D meson in one hemisphere which favours events with no gluon radiation, hence increasing the efficiency for the b-tag in the opposite hemisphere. A comparison between data and Monte Carlo of the spectrum of the most energetic jet in the hemisphere opposite to the D meson has been performed to check the simulation of gluon emission. The quoted error on the correction factors arises from the limited Monte Carlo statistics and the difference between data and Monte Carlo for gluon emission; this gives a relative error on the charm fraction of 0.7%. The relative systematic error due to the uncertainty on the b-tag efficiencies is very small, of the order of 0.2%. The systematics related to the charm fragmentation and the simulation of the decay chain leading to a $D^0$ and $D^+$ are evaluated by varying the fragmentation function and the fraction of charmed vector, pseudoscalar and excited meson (10 to 30%) states produced in the charm hadronisation. The Peterson fragmentation function was varied to reproduce the measured $D^{*+}$ $X_E$ spectrum for different fractions of produced D meson states. Different kinds of fit have been performed to assess the systematic error coming from the fitting. For the signal function, the mean and width of the narrow gaussian distribution is left free, while the relative normalisation and width of the second gaussian is fixed to the Monte Carlo expectation. The fixed parameters have been varied within 5% and the fit repeated with other background parameterisations (second-order polynomial, exponential). Fitting the background outside the mass peak and counting the number of candidates above the mass peak gives a consistent result.

The final result on the $D^0$ and $D^+$ production rate measurements in $Z \to c\bar{c}$ is

$$R_c \times f(c \to D^0) \times B(D^0 \to K^-\pi^+) = (0.370 \pm 0.011 \pm 0.023) \times 10^{-2}$$

$$R_c \times f(c \to D^+) \times B(D^+ \to K^-\pi^+\pi^+) = (0.368 \pm 0.012 \pm 0.020) \times 10^{-2}.$$

Dividing these numbers by the Standard Model value of $R_c$ and the branching fraction for the reconstruction mode, the following fractions are obtained:

$$f(c \to D^0) = 0.559 \pm 0.017 \pm 0.0035 \pm 0.013(\mathrm{BR})$$

and

$$f(c \to D^+) = 0.2379 \pm 0.0077 \pm 0.0129 \pm 0.0190(\mathrm{BR}).$$

The consistency between the rate measurements is investigated. Under the assumption that the observed difference between $f(c \to D^0)$ and $f(c \to D^+)$ is only due to $D^*$ production, i.e. if primary D's and $D^*$'s are produced evenly in the two charge states, the following ratio must equal unity:

$$\frac{f(c \to D^0) - f(c \to D^+)}{2\ f(c \to D^{*+}) \times B(D^{*+} \to D^0\pi^+)}$$

This ratio is measured to be $1.02 \pm 0.12$.

## 7.2 Measurement of the $P_V$ Ratio

The ratio $P_V = \frac{V}{V+P}$, where $V$ is the fraction of $D^*$ (vector) produced and $P$ the fraction of D (pseudoscalar), after all decays of heavier excited states, can be derived either from the ratio $f(c \to D^0)/f(c \to D^+)$, or from the $D^{*\pm}$ and $D^{\pm}$ rates. The latter leads to

$$P_V = 0.595 \pm 0.045.$$

This value is more consistent with the predictions of the thermodynamical approach [18] and the string fragmentation approach of ref. [19], which both predict 0.66 for $P_V$, than from the naive expectation of 0.75 from counting the spin states.

From the analysis of section 6, the $P_V$ ratio is found to be

$$0.60 \pm 0.19.$$

for $D_s^+$ and $D_s^{*+}$ mesons.

## 7.3 Study of $\Lambda_c^+$ and $D_s^+$ production

The c fractions in the $D_s^+$ and $\Lambda_c^+$ samples are extracted by the same method as for the $D^0$ and $D^+$. The background fit includes the Monte-Carlo shape and the proper normalisation of contributions from $D^0$ and $D^+$ to the invariant mass distributions. The efficiency correction is similar, except that the data are counted in 8 $X_E$ bins between 0.2 and 1, allowing the fit of the $X_E$ distributions to a Peterson-based shape for the purpose of extrapolation down to the threshold. The breakdown of the systematic errors is very similar to the one of the previous section and is given in the last two columns of table 6. As the relative $b\bar{b}$ to $c\bar{c}$ contributions are fitted to the data, the uncertainty on the charm fraction is included in the statistical error.

The following $D_s^+$ and $\Lambda_c^+$ product branching ratios in $Z \to c\bar{c}$ are obtained:

$$R_c \times f(c \to D_s^{\pm}) \times B(D_s^+ \to \phi\pi^+) \times B(\phi \to K^+K^-) = (0.352 \pm 0.057 \pm 0.021) \times 10^{-3}$$

$$R_c \times f(c \to \Lambda_c^+) \times B(\Lambda_c^+ \to pK\pi) = (0.673 \pm 0.070 \pm 0.037) \times 10^{-3}.$$

Dividing these numbers by the Standard Model value of $R_c$ and the branching fraction for the reconstruction mode, the following fractions are obtained:

$$f(c \to D_s^+) = 0.116 \pm 0.019 \pm 0.007 \pm 0.030(\mathrm{BR})$$

and

$$f(c \to \Lambda_c^+) = 0.079 \pm 0.008 \pm 0.004 \pm 0.020(\mathrm{BR}).$$

Alternatively, one can use the sum of $R_c \times f(c \to X_c)$ over all the fundamental states of the various hadron species to determine $R_c$ as in section 8.

# 8 Measurement of $R_c$ from Charm Counting

By dividing the values of the product branching fractions found in previous sections by the corresponding decay branching fraction, taken from [14], the following individual charm meson rates are obtained.

$$R_c \times f(c \to D^0) = 0.0961 \pm 0.0029 \pm 0.0060 \pm 0.0023(BR)$$
$$R_c \times f(c \to D^+) = 0.0409 \pm 0.0013 \pm 0.0022 \pm 0.0033(BR)$$
$$R_c \times f(c \to D_s^+) = 0.0199 \pm 0.0032 \pm 0.0012 \pm 0.0050(BR)$$
$$R_c \times f(c \to \Lambda_c^+) = 0.0135 \pm 0.0014 \pm 0.0007 \pm 0.0035(BR)$$

The small additional contribution from $\Xi_c$ and $\Omega_c$ is estimated to be 0.0034 with a 50% uncertainty using usual stangeness suppression factors. Summing all these contributions, a value of

$$R_c = 0.1738 \pm 0.0047(\text{stat.}) \pm 0.0088(\text{syst.}) \pm 0.0075(\text{BR})$$

is found where the systematic uncertainty is a linear sum of the common contributions (nuclear interactions, $dE/dx$, vertexing, gluon splitting, charm fraction and fragmentation), added quadratically to the other contributions. This is in good agreement with the Standard-Model expectation 0.1719 [20] and the accuracy (7%) of this measurement is similar to others [21, 22]. The breakdown of the systematic errors on $R_c$ is given in Table 7.

Table 7: Systematic errors on $R_c$.

| Source | $\delta R_c$ |
|---|---|
| MC statistics | 0.00207 |
| Charm physics | 0.00176 |
| Fragmentation | 0.00599 |
| Charm fraction | 0.00096 |
| Gluon splitting | 0.00051 |
| $dE/dx$ | 0.00156 |
| Nuclear interactions | 0.00087 |
| Vertexing | 0.00516 |
| Mass fits | 0.00177 |
| $B(D^0 \to K^-\pi^+)$ | 0.0023 |
| $B(D^+ \to K^-\pi^+\pi^+)$ | 0.0033 |
| $B(D_s^+ \to \phi\pi^+)$ | 0.0050 |
| $B(\Lambda_c^+ \to pK^-\pi^+)$ | 0.0035 |
| baryons not decaying to $\Lambda_c^+$ | 0.0017 |
| Total internal | 0.0088 |
| Total external | 0.0075 |

# 9 Conclusions

A significant improvement of the knowledge of charm production in Z decays has been achieved. This is due, with respect to previous analyses, to a better rejection of the combinatorial background and a better b/c separation, both coming from the use of the vertex detector. The $D^{*\pm}$ spectrum is measured and interpreted as a sum of three contributions: hadronisation of a charm quark produced in a $Z \to c\bar{c}$ decay, decay of a bottom hadron from a $Z \to b\bar{b}$ decay, and gluon splitting into a pair of heavy quarks which hadronise or decay into a $D^{*\pm}$. This scheme is found to describe the data very well.

The probability for a c quark to hadronise into a $D^{*+}$ meson is found to be

$$f(c \to D^{*+}) = 0.233 \pm 0.010(\text{stat.}) \pm 0.011(\text{syst.}).$$

A fit to the spectrum yields the average fractional energy of the $D^{*\pm}$ in $Z \to c\bar{c}$ events

$$\langle X_E(D^*) \rangle_{c\bar{c}} = 0.4878 \pm 0.0046 \pm 0.0061.$$

Using the heavy - light hemisphere mass difference distribution the average number of gluon splitting events to charm quark pairs per Z hadronic event is found to be

$$\bar{n}_{g \to c\bar{c}} = (3.23 \pm 0.48 \pm 0.53)\%.$$

The production rates of the main charmed ground states have been measured. The effective ratio of Vector/(Vector+Pseudoscalar) production rates in charmed mesons is found to be $0.595 \pm 0.045$, confirming the rather low value found earlier [1], but consistent with recent semi-phenomenological models. For the charmed-strange mesons, a value of $P_V = 0.60 \pm 0.19$ is found.

Summing the contributions of all the fundamental charmed states, and including a contribution from baryons not decaying to $\Lambda_c^+$, a measurement of $R_c$ is achieved:

$$R_c = 0.1738 \pm 0.0047(\text{stat.}) \pm 0.0088(\text{syst.}) \pm 0.0075(\text{BR}).$$

This result, combined with other ALEPH measurements[22], leads to

$$R_c = 0.1698 \pm 0.0069.$$

# Acknowledgements

We wish to thank our colleagues from the accelerator divisions for the successful operation of the LEP machine, and the engineers and technical staff in all our institutions for their contribution to the good performance of ALEPH. Those of us from non-member states thank CERN for its hospitality.

# References


[1] ALEPH Collaboration, *Production of Charmed Mesons in Z Decays*, Z. Phys. C62 (1994) 1.

[2] ALEPH Collaboration, *Measurement of* $\mathrm{D_s^+}$ *Meson Production in Z Decays and of the* $\mathrm{\bar{B}_s^0}$ *Lifetime*, Z. Phys. C69 (1996) 585.

[3] ALEPH Collaboration, *ALEPH: A Detector for Electron-Positron Annihilations at LEP*, Nucl. Instrum. and Methods A294 (1990) 121.

[4] ALEPH Collaboration, *Performance of the ALEPH Detector at LEP*, Nucl. Instrum. and Methods A360 (1995) 481.

[5] ALEPH Collaboration, *A Measurement of* $\mathrm{R_b}$ *using a Lifetime-Mass Tag*, Phys. Lett. B401 (1997) 150.

[6] ALEPH Collaboration, *Update of Electroweak Parameters from Z Decays*, Z. Phys. C60 (1993) 71.

[7] ALEPH Collaboration, *Production of Excited Beauty States in Z Decays*, Z. Phys. C69 (1996) 393.

[8] T. Sjöstrand, Comp. Phys. Commun. 82 (1994) 74.

[9] C. Peterson *et al.*, Phys. Rev. D27 (1983) 105.

[10] ALEPH Collaboration, *Measurement of the* $\mathrm{D^{*\pm}}$ *Cross Section in Two Photon Collisions at LEP*, Phys. Lett. B355 (1995) 595.

[11] ALEPH Collaboration, *A Measurement of the Gluon Splitting Rate into* $\mathrm{b\bar{b}}$ *pairs in Hadronic* Z *Decays*, Phys. Lett. B434 (1998) 437.

[12] G. Marchesini et al., Comp. Phys. Commun. 67 (1992) 465.

[13] L. Lonnblad, Comp. Phys. Commun. 71 (1992) 15.

[14] Particle Data Group, *Review of Particle Physics*, Eur. Phys. Journal C3 (1998) 1. The following branching fractions are used in this paper: $B(\mathrm{D^0} \to \mathrm{K^-\pi^+}) = (3.85 \pm 0.09)\%$, $B(\mathrm{D^+} \to \mathrm{K^-\pi^+\pi^+}) = (9.0 \pm 0.6)\%$, $B(\mathrm{D_s^+} \to \phi\pi^+) = (3.6 \pm 0.9)\%$, $B(\Lambda_c^+ \to \mathrm{pK^-\pi^+}) = (5.0 \pm 1.3)\%$.

[15] OPAL Collaboration, *Measurement of the Multiplicity of Charm Quark Pairs from Gluons in Hadronic* $\mathrm{Z^0}$ *Decays*, Phys. Lett. B353 (1995) 595.

[16] M.H. Seymour, Nucl. Phys B436 (1995) 163.

[17] LEP Collaboration, LEP Electroweak Working Group, SLD Heavy Flavour Group, *A Combination of Preliminary Electroweak Measurements and Constraints on the Standard Model*, CERN–PPE/96-183.

[18] F. Becattini, Z. Phys. C69 (1996) 485.

[19] Yi-Jin Pei, Z. Phys. C72 (1996) 39.

[20] Mark A. Samuel, Phys. Lett. B397 (1997) 241.

[21] DELPHI Collaboration, *A Measurement of* D *Meson Production in* Z *Hadronic Decays,* Z. Phys. C59 (1993) 533.
OPAL Coll., *A Study of Charm Hadron Production in* $Z \to c\bar{c}$ *and* $Z \to b\bar{b}$ *Decays at LEP,* Z. Phys. C72 (1996) 1.

[22] ALEPH Collaboration, *Measurement of the fraction of hadronic Z decays into charm quark pairs*, Eur. Phys. Journal C4 (1998) 387.